Supplementary Information

An AND-gated drug and photoactivatable Cre-loxP system for spatiotemporal control in cell-based therapeutics

Molly E. Allen[1,2], Wei Zhou[3], Jeyan Thangaraj[1,2], Phillip Kyriakakis[1], Yiqian Wu[1,2], Ziliang Huang[1,2], Phuong Ho[1,2], Yijia Pan[1,2], Praopim Limsakul[1,2], Xiangdong Xu[4*], and Yingxiao Wang[1,2*]

[1]Department of Bioengineering, [2]Institute of Engineering in Medicine, University of California, San Diego, 9500 Gilman Drive, La Jolla, California 92093-0412, United States, [3]Chongqing Cancer Hospital, 181 Hanyu Road, Shapingba District, Chongqing 400030, China, [4]Department of Pathology, Veterans Affairs San Diego Healthcare System, University of California, San Diego, 9500 Gilman Drive, La Jolla, California 92093-0412, United States

Corresponding Authors:
Yingxiao Wang, Ph.D., Email: yiw015@ucsd.edu, Tel: 858-534-5256
Xiangdong Xu, M.D., Ph.D., Email: xxu@ucsd.edu, Tel: 858-642-1415

Table of Contents

Supplementary Table S1. Truth table highlighting potential on-target off-tumor toxicity risks for several engineered CAR T cell system. CAR T cell systems target localized cancerous cells that express Antigen1 and/or Antigen2. Expected CAR-mediated T cell activation is given as an output for each unique combination of inputs, noting incidents of on-target on-tumor (blue) and on-target off-tumor toxicities (red). Blue light stimulation is only applied locally at the tumor site. T cells expressing the basic α-Antigen1 CAR will trigger on-target off-tumor toxicity against any Antigen1$^+$ healthy cells along with cancer cells. The ON-Switch α-Antigen1 CAR system[1] relies on a diffusible small molecule to restore CAR function. Small molecules, however, are at risk of diffusing throughout the body, leaving Antigen1$^+$ healthy cells susceptible to on-target off-tumor toxicity. The cytosolic costimulatory and activating domains of CAR can be split into 2 proteins, each with a unique antigen recognition domain. CAR function is restored upon binding to Antigen1$^+$ Antigen2$^+$ targeted cancer cells.[2] However, the split CAR will also trigger on-target off-tumor toxicity against any Antigen1$^+$ Antigen2$^+$ healthy cells. The synNotch receptor localizes T cells to all Antigen1$^+$ cells, after which α-Antigen2 CAR is automatically expressed,[3] similarly risking on-target off-tumor toxicity against Antigen1$^+$ Antigen2$^+$ healthy cells. The TamPA-Cre system localizes T cells to all Antigen1$^+$ cells, but α-Antigen2 CAR is only expressed after global tamoxifen administration and localized blue light stimulation. As long as Antigen1$^+$ Antigen2$^+$ healthy cells are not colocalized with cancer cells, they are not at risk for on-target off-tumor toxicity.

	Input(s)				Output: CAR-Mediated T Cell Activation On-target On-tumor or On-target Off-tumor				
	Antigen1$^+$ Target	Antigen2$^+$ Target	Small Molecule Stimulation	Blue Light Stimulation	α-Antigen1 CAR	ON-Switch α-Antigen1-CAR	α-Antigen1, α-Antigen2 Split CAR	α-Antigen1 synNotch α-Antigen2 CAR	TamPA-Cre α-Antigen1 Receptor α-Antigen2 CAR
Healthy Cells	0	0	0	0	0	0	0	0	0
	0	0	1	0	0	0	0	0	0
	0	1	0	0	0	0	0	0	0
	0	1	1	0	0	0	0	0	0
	1	0	0	0	1	0	0	0	0
	1	0	1	0	1	1	0	0	0
	1	1	0	0	1	0	1	1	0
	1	1	1	0	1	1	1	1	0
Cancer Cells	1	1	0	0	1	0	1	1	0
	1	1	0	1	1	0	1	1	0
	1	1	1	0	1	1	1	1	0
	1	1	1	1	1	1	1	1	1

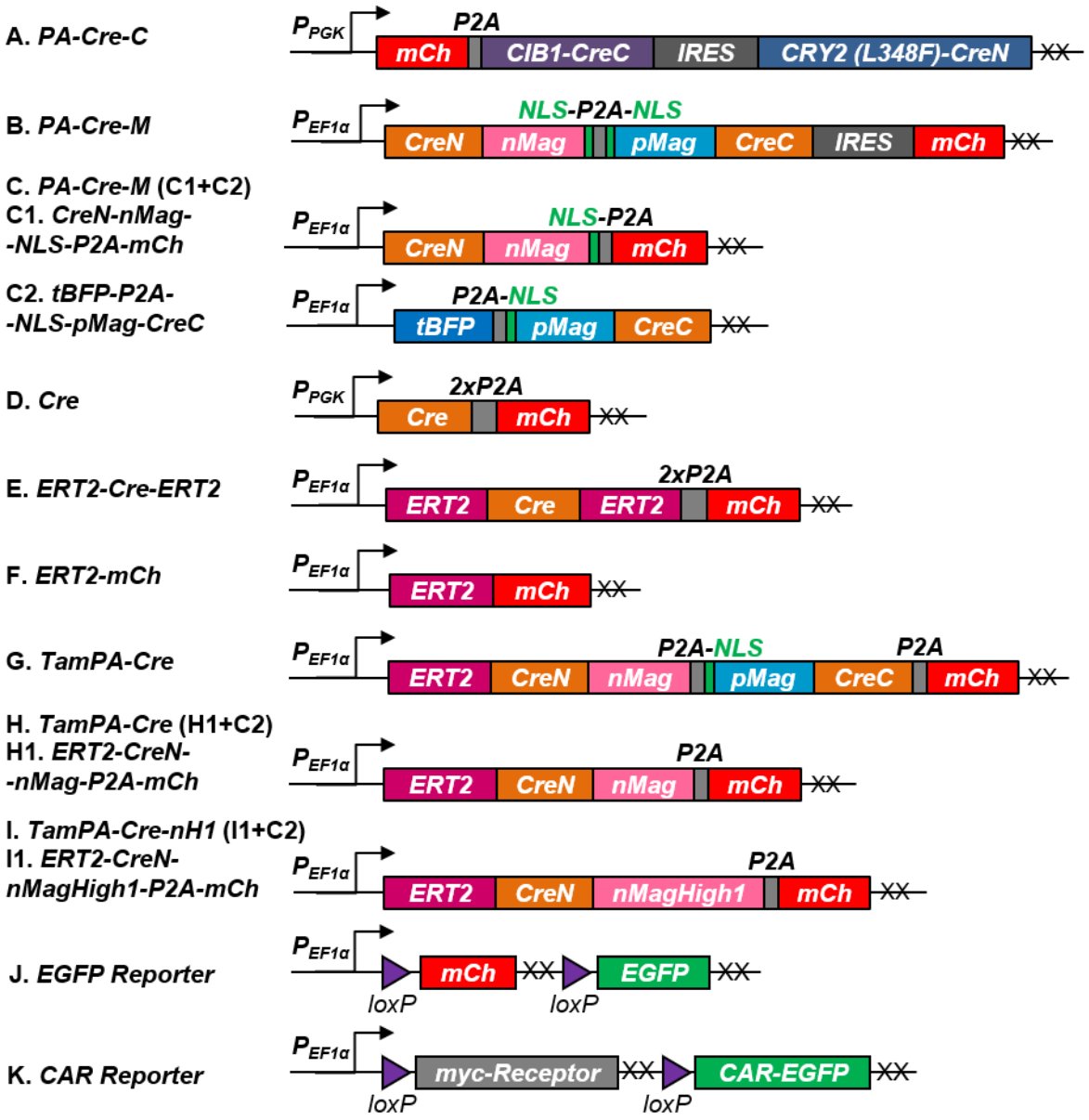

Figure S1. Schematic representations of genetic constructs. The following constructs were assembled as detailed in the "Supplementary-Constructs-Spreadsheet" file: (A, pMA002) PA-Cre-C:[4] *pSin-mPGK-mCherry-P2A-CIB1CreC(106-343)-IRES-CRY2(L348F)CreN(19-104);* (B, pMA005) PA-Cre-M[5] in one vector: *pSin-hEF1α-CreN(19-59)-NLS-P2A-NLS-dpMag-CreC(60-343);* or (C) in two vectors: (C1, pMA003) *pSin-hEF1α-CreN(19-59)-nMag-NLS-P2A-mCherry-IRES-PuroR* and (C2, pMA004) *pSin-hEF1α-tBFP-P2A-NLS-pMag-CreC(60-343)-IRES-PuroR;* (D, pMA001) Cre: *pSin-hEF1α-Cre-2xP2A-mCherry*; (E, pMA006) ERT2-Cre-ERT2: *pSin-hEF1α-ERT2-Cre-ERT2*; (F, pMA007) ERT2-mCh: *pSin-hEF1α-ERT2-mCherry*; (G, pMA013) TamPA-Cre in one vector: *pSin-hEF1α-ERT2-CreN(2-59)-nMag-P2A-NLS-dpMag-CreC(60-343)-P2A-mCherry*; or (H) in two vectors: (H1, pMA011) *pSin-hEF1α-ERT2-CreN(2-59)-nMag-P2A-mCherry-IRES-PuroR* and (C2, pMA004); (I) TamPA-Cre-nH1 in two vectors: (I1, pMA012) *pSin-hEF1α-ERT2-CreN(2-59)-nMagHigh1-IRES-PuroR* and (C2, pMA004); (J, pMA014) EGFP Reporter: *pSin-hEF1α-loxp-mCherry-2stop-loxP-EGFP-IRES-PuroR*; (K, pMA022) CAR Reporter *pSin-hEF1α-loxp-myc-α-CD38-Receptor-2stop-loxP-α-CD19-CAR-EGFP-IRES-PuroR*. dpMag = codon diversified pMag (see Fig. S4).

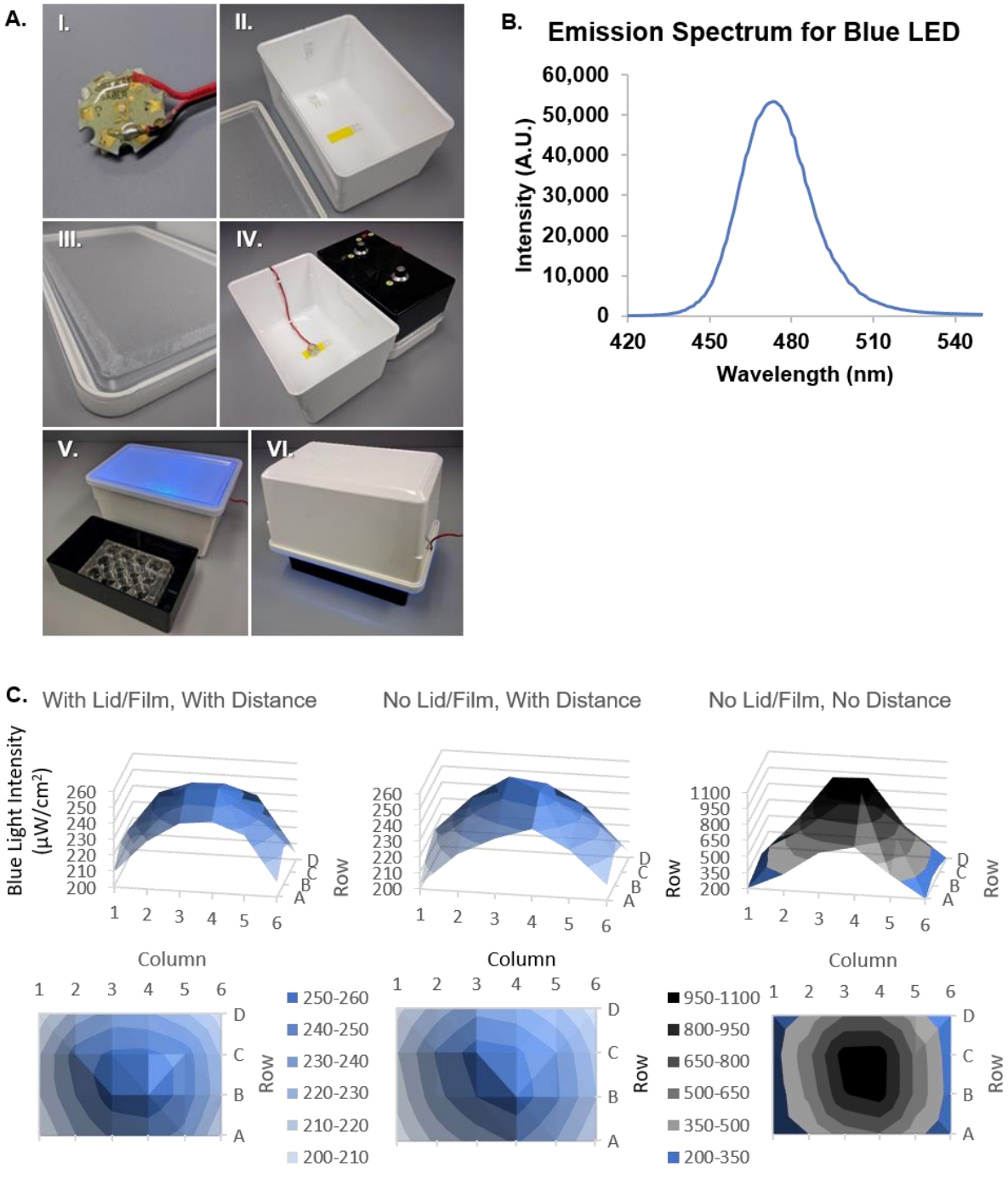

Figure S2. Design and characterization of the blue light stimulation apparatus. (A) To distribute light from a single LED evenly across a standard 24-well plate of cells, we built the blue light stimulation apparatus with an LED placed at a defined distance from a polypropylene light-diffusion film. (I) Close up of the mounted blue LED covered in a protective layer of transparent epoxy. (II) Dual Lock Reclosable Fasteners (3M, yellow) were adhered to the back of the LED (not shown) and in the center bottom of a deep, polyester white-walled container with a clear PET plastic lid and synthetic rubber gasket. Small plastic Decorating Clips (Command, white) were used to hold the LED wire along the inner walls of the container, out of the light path. A small notch was cut into the white container to minimize strain on the wire when the lid was fastened. (III) A polypropylene

Figure S2. Design and characterization of the blue light stimulation apparatus Continued. static-cling frosted window film was cut to size and placed on the inside of the lid to work as a light-diffusion film. (IV) The LED was mounted in the bottom center of the container and the wires secured with clips. In the background, the wire connects to the intensity-adjustable blue LED control system (Phillip Kyriakakis). (V) The lid was fastened onto the blue light box and the blue light is turned on to demonstrate function. The cell culture place was centered inside a lidless black plastic box, which was fitted to the beveled lid of the blue light box (VI) After blue light intensity was measured and adjusted using a power meter, the blue light box was flipped upside down and centered on top of the cell culture plate in the lidless black plastic box. During experiments, this configuration is assembled inside of a humidified 37°C, 5% CO_2 cell culture incubator. Finally, blue light exposure times and patterns are entered into the LED control system's LabVIEW-based software outside of the incubator. (B) Spectral evaluation of the blue LED used to stimulate photoactivatable Cre-*loxP* recombination. The LED was measured by mounting it onto a cell culture plate, then using a microplate reader (Infinite M1000 Pro, Tecan) to measure the intensity of the LED at different wavelengths (1 nm intervals). Peak intensity wavelength occurred at 473 nm (bandwidth = 29 nm). (C) Characterization of light distribution showing more even distribution with greater distance from the LED light and with scattering from the diffusion film lid. The blue light box was set up shown in A-VI, such that light intensity could be measured at the approximate location experience by cells in each well of a 24-well plate. The shortest distance between the light source and center of the 24-well plate cell culture plane was approximately 15.5 cm. The lid with the diffusion filter was located a minimum of 10.1 cm from the light source. Future designs will include an array of multiple LEDs to further improve light distribution.

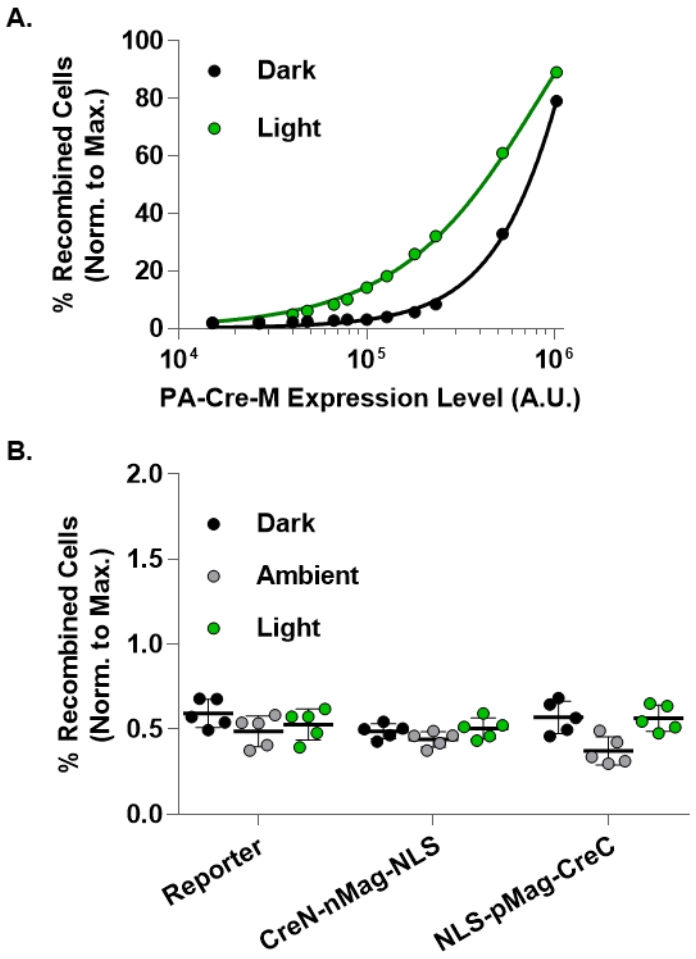

Figure S3. Additional characterization of the PA-Cre-M system. (A) Excessive expression of PA-Cre-M drives high levels of spontaneous recombination. CAR Reporter Jurkat T cells were transiently transfected via electroporation with PA-Cre-M (Fig. S1C). 24-hours post-transfection, cells were (Light) or were not (Dark) subjected to pulsatile blue light stimulation for 24h (50 W/m^2, 1s per min). Trend lines fitted to Dark (black) and Light (green) groups were created using a two-phase exponential association model (See Table S2). At low PA-Cre-M expression levels (as measured by the intensity of the mCherry marker), the difference between the Light and Dark groups is small. With increasing expression level, light-induced PA-Cre-M drives increasing levels of recombination while cells kept in the dark remain relatively low. However, at higher expression levels, the difference between Recombination in Dark and Light groups begins to narrow as cells in the Dark groups become more susceptible to spontaneous background recombination. Data is from the analysis of one experiment, but represents a common trend seen across several different experiments in which PA-Cre-M was variably expressed. (B) Cre-*loxP* recombination cannot be driven by CreN-nMag-NLS or NLS-pMag-CreC alone. EGFP Reporter HEK293T cells transiently transfected with CreN-nMag-NLS-P2A-mCherry (CreN-nMag-NLS), or tBFP-P2A-NLS-pMag-CreC (NLS-pMag-CreC) constructs either were (Light) or were not (Dark, Ambient) exposed to blue light stimulation (5 W/m^2, 7.5s per min, 24h) (n=5). Across Reporter, CreN-nMag-NLS, and NLS-pMag-CreC groups, there is no significant difference seen in any light condition (Dark, Ambient, Light). Blue light stimulation started and flow cytometry measurements taken 24h and 72h post-transfection, respectively. Percentage of recombined HEK293T cells (normalized to maximal recombination) = 100%*(% of EGFP$^+$ cells) / (mean % of EGFP$^+$ cells in corresponding Cre groups).

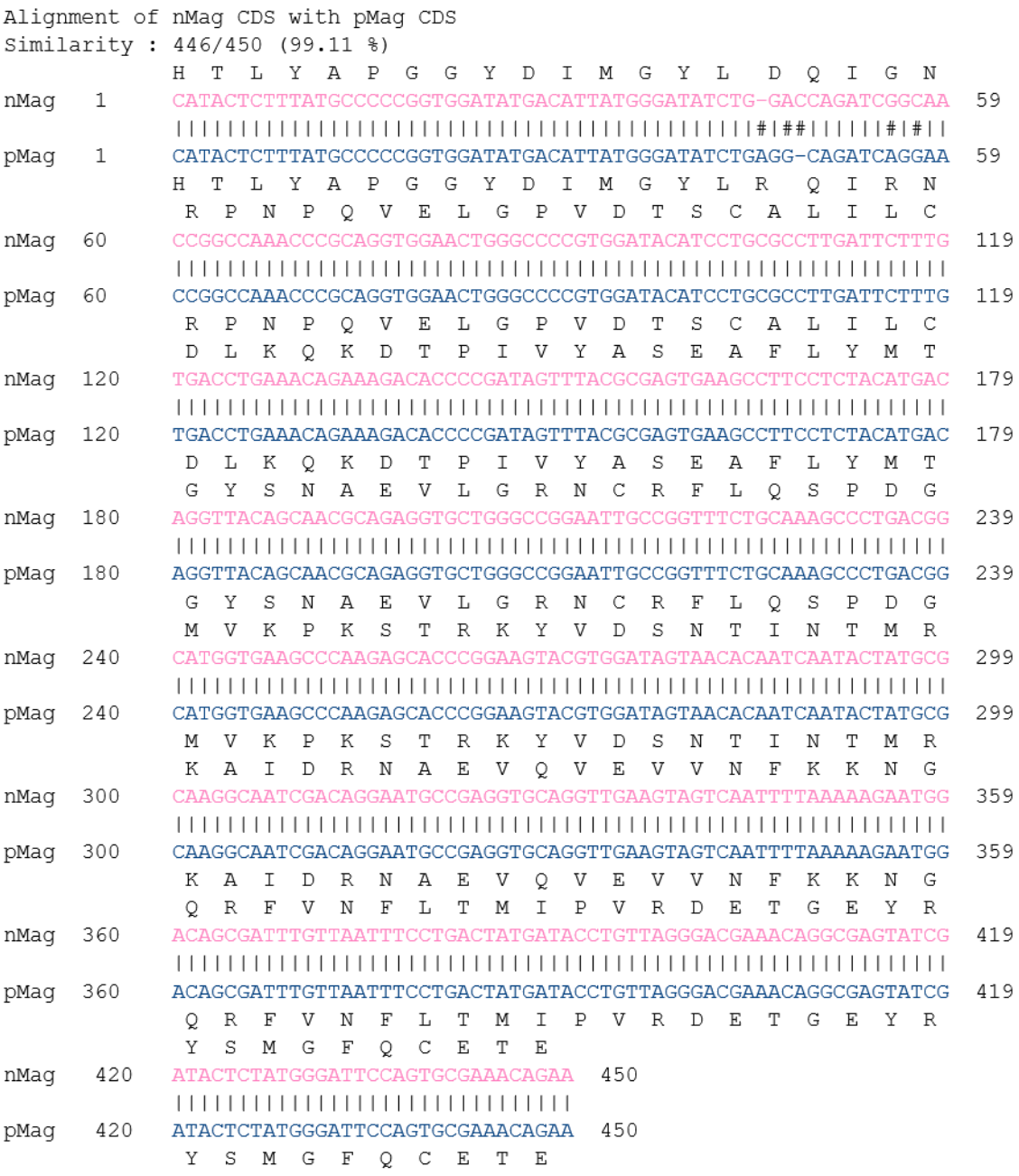

Figure S4. Diversification of the pMag CDS. (A) DNA sequence alignment of nMag and pMag (Serial Cloner 2.6.1) from PA-Cre-M[5] showing that the CDS for each are nearly identical and are thus susceptible potential recombination introduced by lentiviral gene transfer.[6] (B) DNA sequence alignment of pMag with codon-diversified dpMag (Serial Cloner 2.6.1). Reduced sequence similarity helps prevent potential recombination introduced by lentiviral gene transfer.[6] Codon diversification of the pMag CDS was done by hand and synthesized dpMag dsDNA (Integrated DNA Technologies) was used for subsequent molecular cloning.

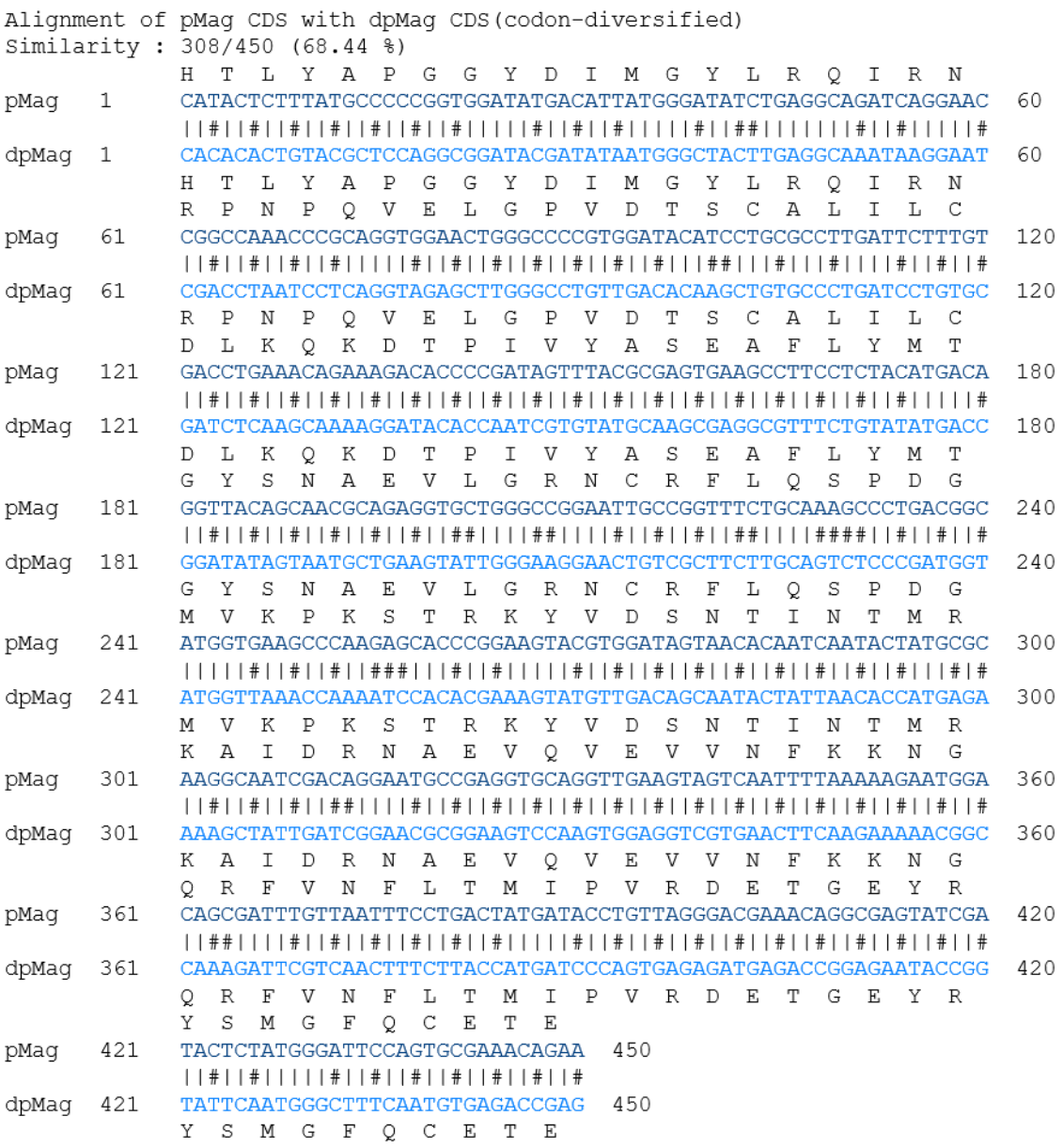

Figure S4. Diversification of the pMag CDS Continued.

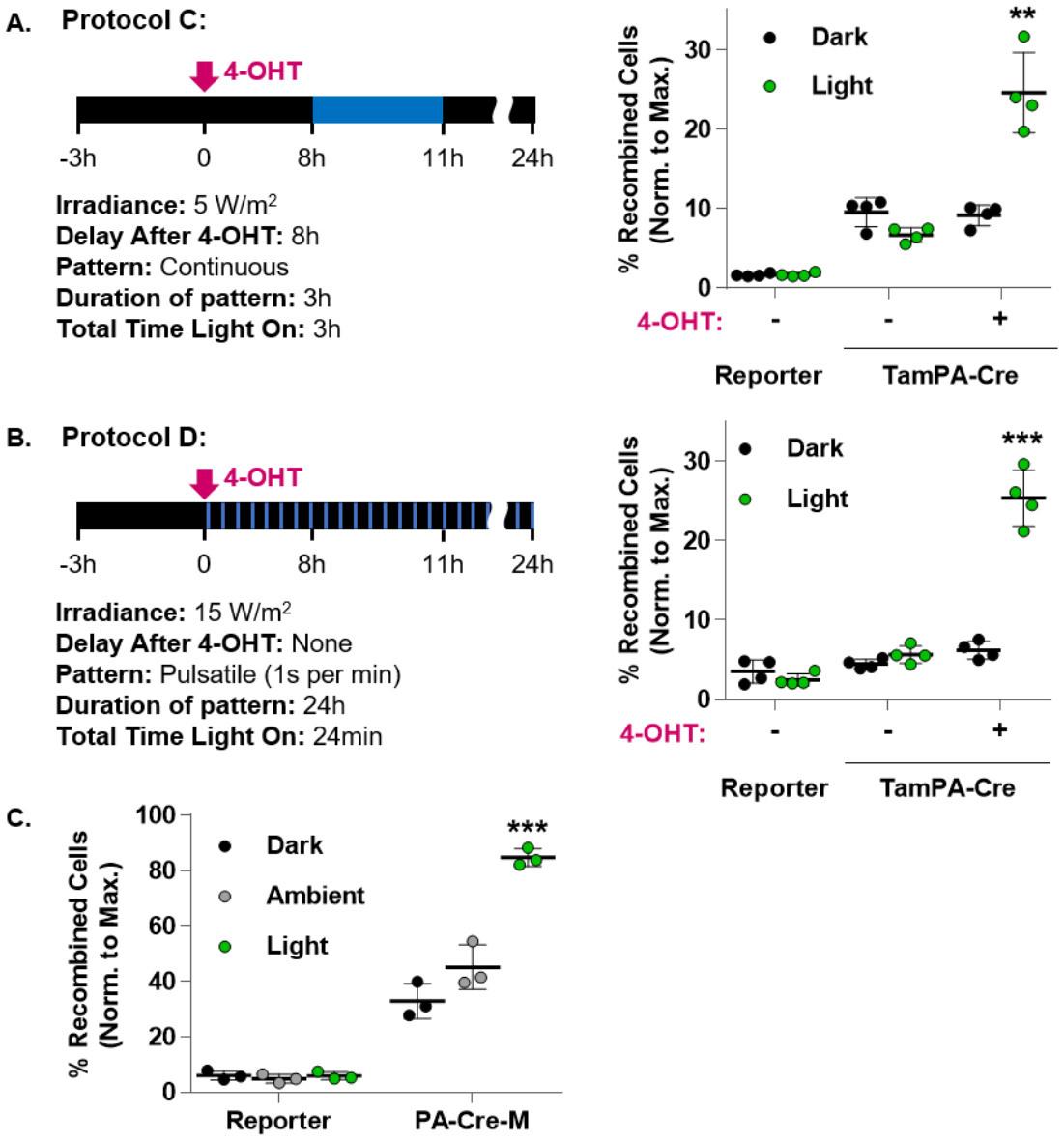

Figure S5. Optimizing TamPA-Cre recombination efficiency through different tamoxifen and blue light stimulation protocols. (A,B) Schematic illustrating the tamoxifen and blue light stimulation protocols and the normalized percentage of recombined EGFP Reporter HEK293T cells transiently transfected with TamPA-Cre or Cre constructs that were (Light) or were not (Dark) exposed to blue light stimulation outlined in (A) Protocol C: (5 W/m², 3h) started 8h after 4-OHT addition (n=4), or (B) Protocol D: (15 W/m², 7.5s per min, 24h) started with 4-OHT addition. Delaying blue light stimulation after 4-OHT addition and changing to a pulsatile blue light pattern improved TamPA-Cre performance. (C) For comparison, EGFP Reporter HEK293T cells transiently transfected with PA-Cre-M or Cre constructs were (Light) or were not (Dark, Ambient) exposed to Protocol B: (5 W/m², 7.5s per min, 24h) started 3h after 4-OHT addition (n=3). Reporter = untransfected EGFP Reporter HEK293T cell line. Blue light stimulation started and flow cytometry measurements taken 24h and 72h post-transfection, respectively. Percentage of recombined HEK293T cells (normalized to maximal recombination) = 100%*(% of EGFP⁺ cells) / (mean % of EGFP⁺ cells in corresponding Cre groups).

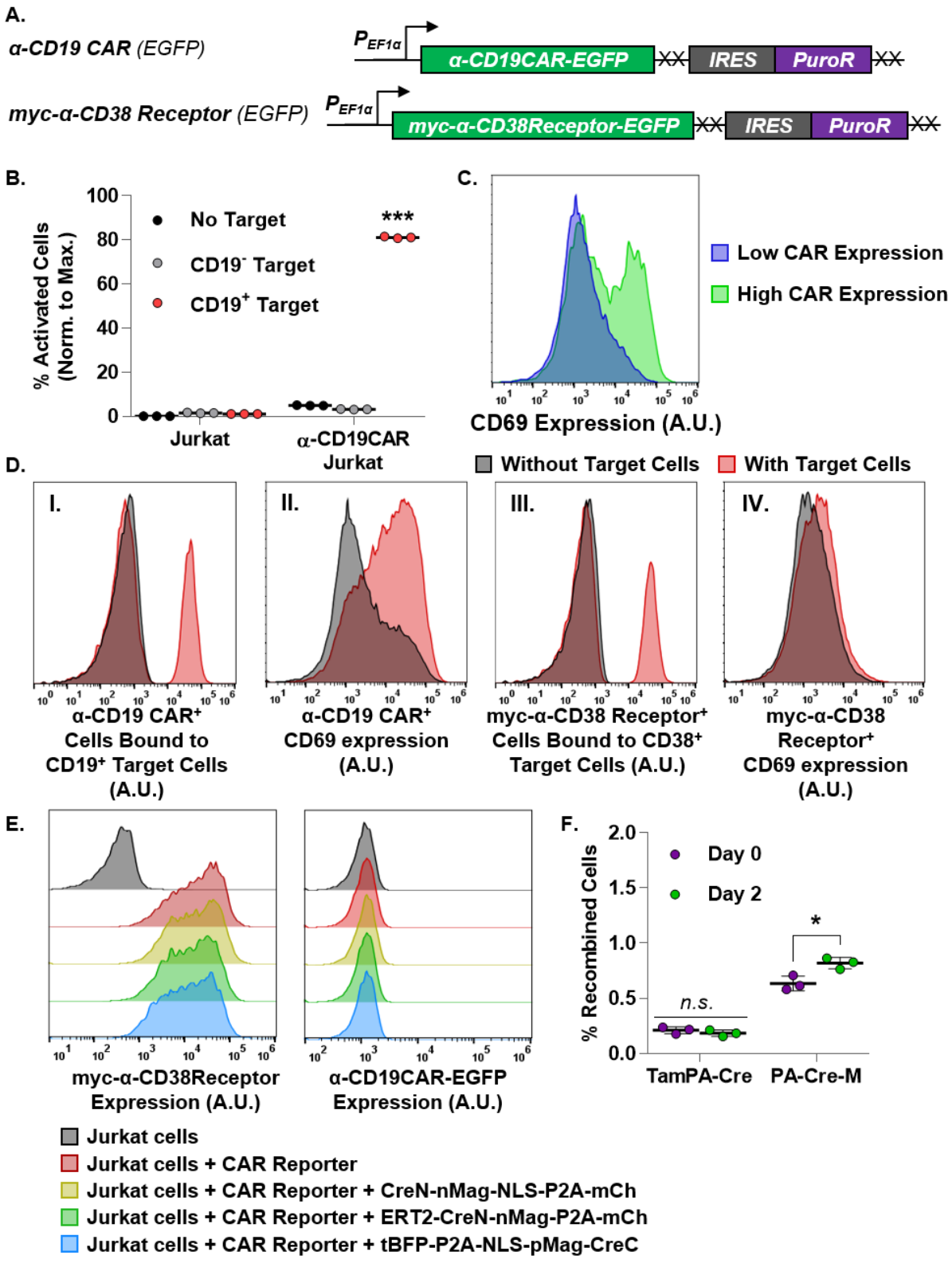

Figure S6. CAR-mediated T cell activation is antigen specific at low CAR expression levels. (A) Schematic representation of the *α-CD19CAR-EGFP* (pMA017) and the *myc-α-CD38Receptor-EGFP* (pMA020) genetic constructs. The hEF1α promoter drives constitutive expression of *α-CD19CAR* or *myc-α-CD38Receptor* (*pSin-*

hEF1α-α-CD19-CAR-ggsggt-EGFP-IRES-PuroR, or *pSin-hEF1α-myc-α-CD38Receptor-ggsggt-EGFP-IRES-PuroR*, respectively). (B) Jurkat T cells and α-CD19-CAR-EGFP$^+$ Jurkat T cells were co-incubated with an equal number of either CD19$^-$ K562 Target cells, CD19$^+$ Toledo Target cells, or no Target cells for 24h after which the normalized percentage of activated (% CD69$^+$) Jurkat T cells was measured via flow cytometry (n=3). Only α-CD19CAR$^+$ Jurkat T cells co-incubated with CD19$^+$ Toledo Target cells were significantly activated (81.1 ± 0.35 %). Co-incubation with either no Target cells or CD19$^-$ K562 Target cells yielded similar results, indicating that CAR-mediated T cell activation is not affected by the presence or absence of TAA$^-$ Target cells. (C) Representative histograms from flow cytometry showing that a greater portion of Jurkat T cells expressing high levels of α-CD19-CAR-EGFP undergo non-specific T cell activation in culture (CD69$^+$, green) compared to those expressing low levels of α-CD19-CAR-EGFP (blue). (D) Representative histograms from flow cytometry showing that α-CD19-CAR-EGFP$^+$ Jurkat T cells both (I) bind to and (II) are activated by CD19$^+$ Toledo Target cells, while myc-α-CD38-Receptor$^+$ Jurkat T cells (III) bind to but (IV) are not activated by CD38$^+$ Toledo Target cells. (E) Representative histograms from flow cytometry measurement of CAR Reporter Jurkat cell line (red) transduced with either CreN-nMag-NLS-P2A-mCh (yellow), ERT2-CreN-nMag-P2A-mCh (green), or tBFP-P2A-NLS-pMag-CreC (blue) constructs. All CAR Reporter Jurkat T cells express myc-α-CD38Receptor (left) and do not express α-CD19-CAR-EGFP (right). Non-transduced Jurkat T cells (black) are shown for reference. (F) PA-Cre-M$^+$ and TamPA-Cre$^+$ CAR Reporter Jurkat cell lines were exposed to the Ambient light condition. The percentage of recombined cells (% CAR-EGFP$^+$) was measured before and after via flow cytometry (n=3). After 48h, PA-Cre-M had driven a significant increase in recombination while no such change was seen in TamPA-Cre groups. This increase in PA-Cre-M groups is likely due to a combination of spontaneous and ambient light-driven recombination. Reporter = CAR Reporter Jurkat T cell line. Recombination = % CAR-EGFP$^+$ cells, and Activation = % CD69$^+$ cells, where 100% represents maximal recombination efficiency. Percentage of recombined Jurkat T cells (normalized to maximal recombination) = 100%*(% of CAR-EGFP$^+$ cells) / (initial % of CAR Reporter$^+$ cells, measured via myc).

A.

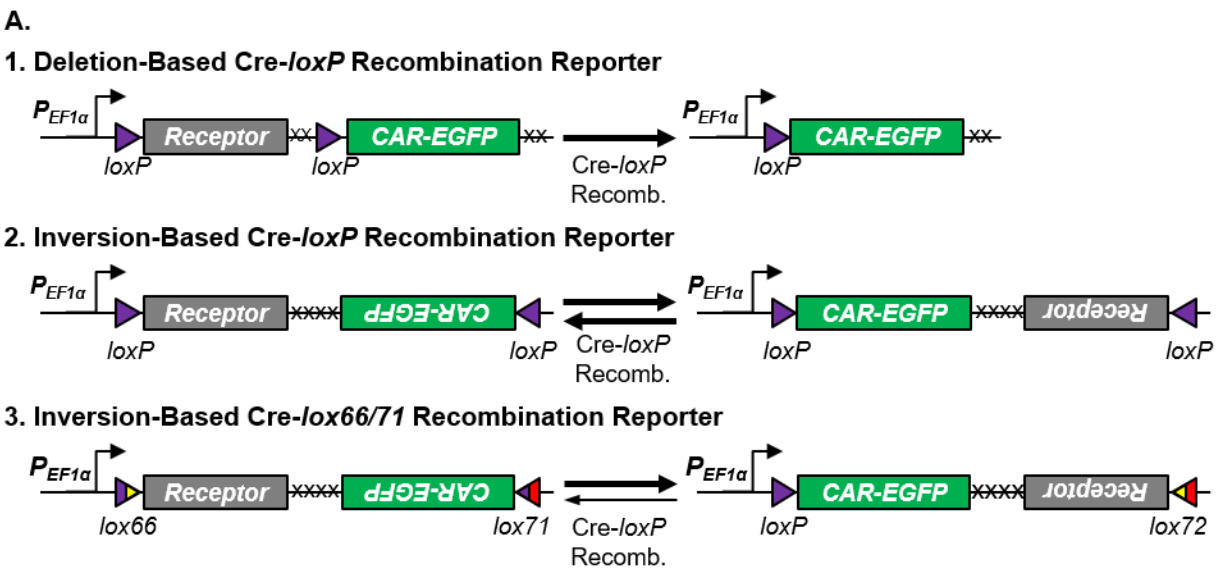

B.

	1. Cre-*loxP* Deletion		2. Cre-*loxP* Inversion		3. Cre-*lox66/71* Inversion	
Recombination	**Irreversible**		**Reversible**		**Mostly Irreversible**	
Pre-recombination fraction of CAR⁺ cells	+ +	(high copy)	-	(high copy)	-	(high copy)
	-	(low copy)	-	(low copy)	-	(low copy)
Post-recombination fraction of CAR⁺ cells	+ + + +	(high copy)	+ +	(high copy)	+ + +	(high copy)
	+ + + +	(low copy)	+ +	(low copy)	+ + +	(low copy)
Post-recombination CAR expression level	+ + + +	(high copy)	+ +	(high copy)	+ +	(high copy)
	+ +	(low copy)	+	(low copy)	+	(low copy)

Figure S7. Testing different Cre-*loxP* CAR Reporter designs. (A) Three different Cre-*loxP* CAR Reporter constructs were evaluated: (1) deletion-based (irreversible), (2) inversion-based (reversible), and (3) inversion based with *loxP* mutant sites lox66 and lox71 (mostly irreversible). (B) Qualitative summary of Cre-, PA-Cre-, and TamPA-Cre-mediated recombination experiments that were conducted in both HEK293T and Jurkat T cells expressing high (high copy) or low (low copy) levels of each CAR Reporter construct. While inversion-based CAR Reporters had the advantage of preventing all background CAR-EGFP expression before recombination, the deletion-based CAR Reporter functioned similarly at low copy number while providing more robust expression levels of CAR-EGFP after recombination. In the ideal CAR Reporter design, the receptor would continue to be expressed after recombination. However, due to lentiviral packaging size constraints and a desire to minimize the number of individually introduced components, only one promoter could be used. As efficiency improves, other gene insertion methods (e.g. CRISPR-Cas9) will undoubtedly allow for larger, more complex designs.

A. $$A(t) = A_0 * 2^{-\left(\frac{t}{k}\right)} = A_0 * 2^{-\left(\frac{t}{1.8h}\right)} = A_0 * 2^{-\left(\frac{t}{6{,}480s}\right)}$$

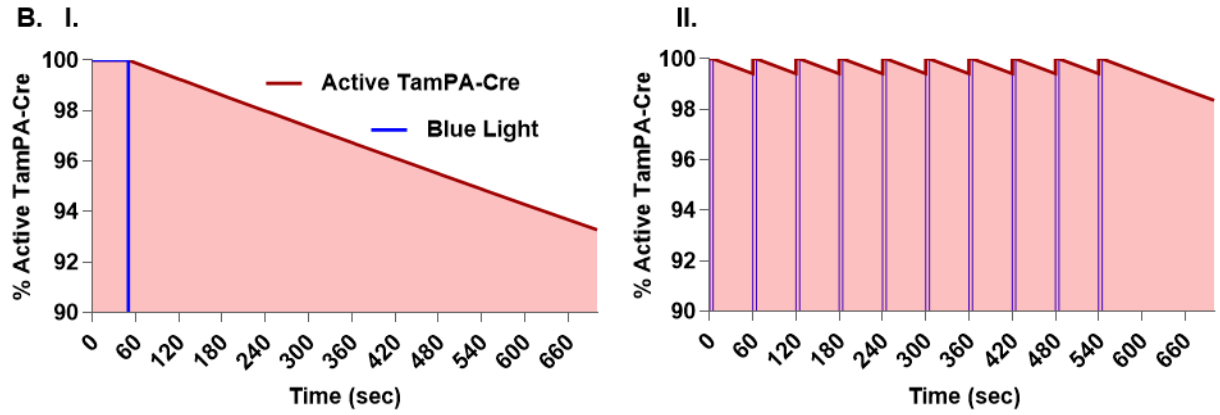

Figure S8. Pulsatile blue light stimulation protocols improve Cre-*loxP* recombination efficiency due to slow nMag-pMag dissociation kinetics. (A) Blue light-induced heterodimerization between nMag and pMag proteins occurs rapidly, but nMag-pMag heterodimers dissociate exponentially with a half-life of ~1.8h upon the removal of light.[7] From an initial heterodimer concentration of A_0, the remaining heterodimer concentration after the blue light stimulus is removed can be calculated as a function of time using the exponential decay equation, where the half-life k is equal to 1.8h (6,480s). Such slow degradation kinetics maintain the percentage of active TamPA-Cre above 99.0% up to 93s after blue light is removed. (B) The plots track the theoretical percentage of active TamPA-Cre in tamoxifen-induced cells given (I) 50s of continuous blue light stimulation or given (II) ten 5-second pulses of (equivalent intensity) blue light stimulation, each pulse separated by 55s of darkness (a shortened version of Protocol E, Fig. 4C). 700s after the beginning of each blue light stimulation protocol, only 93.28% of maximal active TamPA-Cre levels remain given 10s of continuous light, while 98.36% of maximal active TamPA-Cre is still present to drive recombination given the pulsatile protocol. The area under the % Active TamPA-Cre curve (shaded red) is proportional to the probability that a given cell will undergo Cre-*loxP* recombination over a given time interval. From these graphs, it is obvious that the area under to curve for the pulsatile blue light stimulation (II) is greater than for continuous blue light stimulation (I), thus increasing the chances that these cells will undergo TamPA-Cre-mediated Cre-*loxP* recombination.

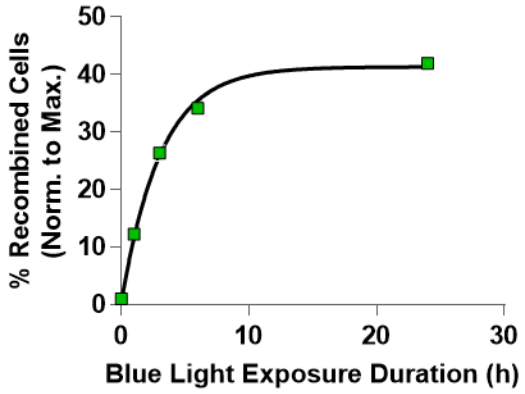

Figure S9. Cre-*loxP* recombination in TamPA-Cre$^+$ CAR Reporter Jurkat T cells plateaus between 6h and 24h of blue light stimulation. Alternate graphical representation of Figure 4D with non-linear fit exponential growth trendline (See Table S2). Percentage of recombined Jurkat T cells (normalized to maximal recombination) = 100%*(% of CAR-EGFP$^+$ cells) / (initial % of CAR Reporter$^+$ cells, measured via myc).

Table S2. Non-linear Fit Trendline Information. Parameters of non-linear fit trendlines in Fig. S3, S9, and 4E (GraphPad Prism 7.04).

Non-linear Fit for Fig. S3 (Dark)	
Two phase exponential association	Y=Ymax1*(1-exp(-K1*X)) + Ymax2*(1-exp(-K2*X))
Best-fit values	
Ymax1	~ 1395
K1	~ 8.632e-007
Ymax2	~ -1116
K2	~ 1.061e-006
HalfLife_1	~ 803039
HalfLife_2	~ 653400
Std. Error	
Ymax1	~ 1347390
K1	~ 0.0001031
Ymax2	~ 1351367
K2	~ 0.0001136
95% CI (profile likelihood)	
Ymax1	(Very wide)
K1	(Very wide)
Ymax2	(Very wide)
K2	(Very wide)
HalfLife_1	
HalfLife_2	
Goodness of Fit	
Degrees of Freedom	8
R square	0.9979
Absolute Sum of Squares	11.74
Sy.x	1.211
Constraints	
K1	K1 > 0
K2	K2 > 0
Number of points	
# of X values	48
# Y values analyzed	12

Non-linear Fit for Fig. S3 (Light)	
Two phase exponential association	Y=Ymax1*(1-exp(-K1*X)) + Ymax2*(1-exp(-K2*X))
Best-fit values	
Ymax1	~ 91.95
K1	~ 1.241e-006
Ymax2	~ 32.57
K2	~ 1.242e-006
HalfLife_1	~ 558449
HalfLife_2	~ 558143
Std. Error	
Ymax1	~ 25035263861847
K1	~ 92.78
Ymax2	~ 25035263863047
K2	~ 261.2
95% CI (profile likelihood)	
Ymax1	(Very wide)
K1	(Very wide)
Ymax2	(Very wide)
K2	(Very wide)
HalfLife_1	
HalfLife_2	
Goodness of Fit	
Degrees of Freedom	8
R square	0.9982
Absolute Sum of Squares	14
Sy.x	1.323
Constraints	
K1	K1 > 0
K2	K2 > 0
Number of points	
# of X values	48
# Y values analyzed	12

Table S2. Non-linear Fit Trendline Information, Continued.

Non-linear Fit for Fig. S9	
One phase exponential association	Y=Ymax*(1-exp(-K*X))
Best-fit values	
Ymax	0.413
K	0.3253
HalfLife	2.131
Std. Error	
Ymax	0.005569
K	0.01258
95% CI (profile likelihood)	
Ymax	0.4012 to 0.4251
K	0.2992 to 0.3546
HalfLife	1.955 to 2.317
Goodness of Fit	
Degrees of Freedom	18
R square	0.9942
Absolute Sum of Squares	0.002519
Sy.x	0.01183
Constraints	
K	K > 0
Number of points	
# of X values	20
# Y values analyzed	20
Non-linear Fit for Fig. 4E (% myc-Receptor$^+$ Cells)	
One phase exponential decay	Y=Span*exp(-K*X) + Plateau
Best-fit values	
Span	= 1.026
K	0.542
Plateau	0.02641
HalfLife	1.279
Std. Error	
K	0.1417
Plateau	0.07495
95% CI (profile likelihood)	
K	0.3583 to 0.7395
Plateau	-0.1024 to 0.1169
HalfLife	0.9373 to 1.934

Non-linear Fit for Fig. 4E (% myc-Receptor$^+$ Cells) Continued	
Goodness of Fit	
Plateau	-0.1024 to 0.1169
HalfLife	0.9373 to 1.934
Goodness of Fit	
Degrees of Freedom	10
R square	0.9571
Absolute Sum of Squares	0.03617
Sy.x	0.06014
Constraints	
Span	Span = 1.026
K	K > 0
Number of points	
# of X values	12
# Y values analyzed	12
Non-linear Fit for Fig. 4E (% CAR-EGFP$^+$ Cells)	
One phase exponential association	Y=Ymax*(1-exp(-K*X))
Best-fit values	
Ymax	0.4643
K	1.251
HalfLife	0.554
Std. Error	
Ymax	0.008901
K	0.102
95% CI (profile likelihood)	
Ymax	0.4446 to 0.4851
K	1.039 to 1.523
HalfLife	0.455 to 0.6673
Goodness of Fit	
Degrees of Freedom	10
R square	0.8925
Absolute Sum of Squares	0.004884
Sy.x	0.0221
Constraints	
K	K > 0
Number of points	
# of X values	12
# Y values analyzed	12

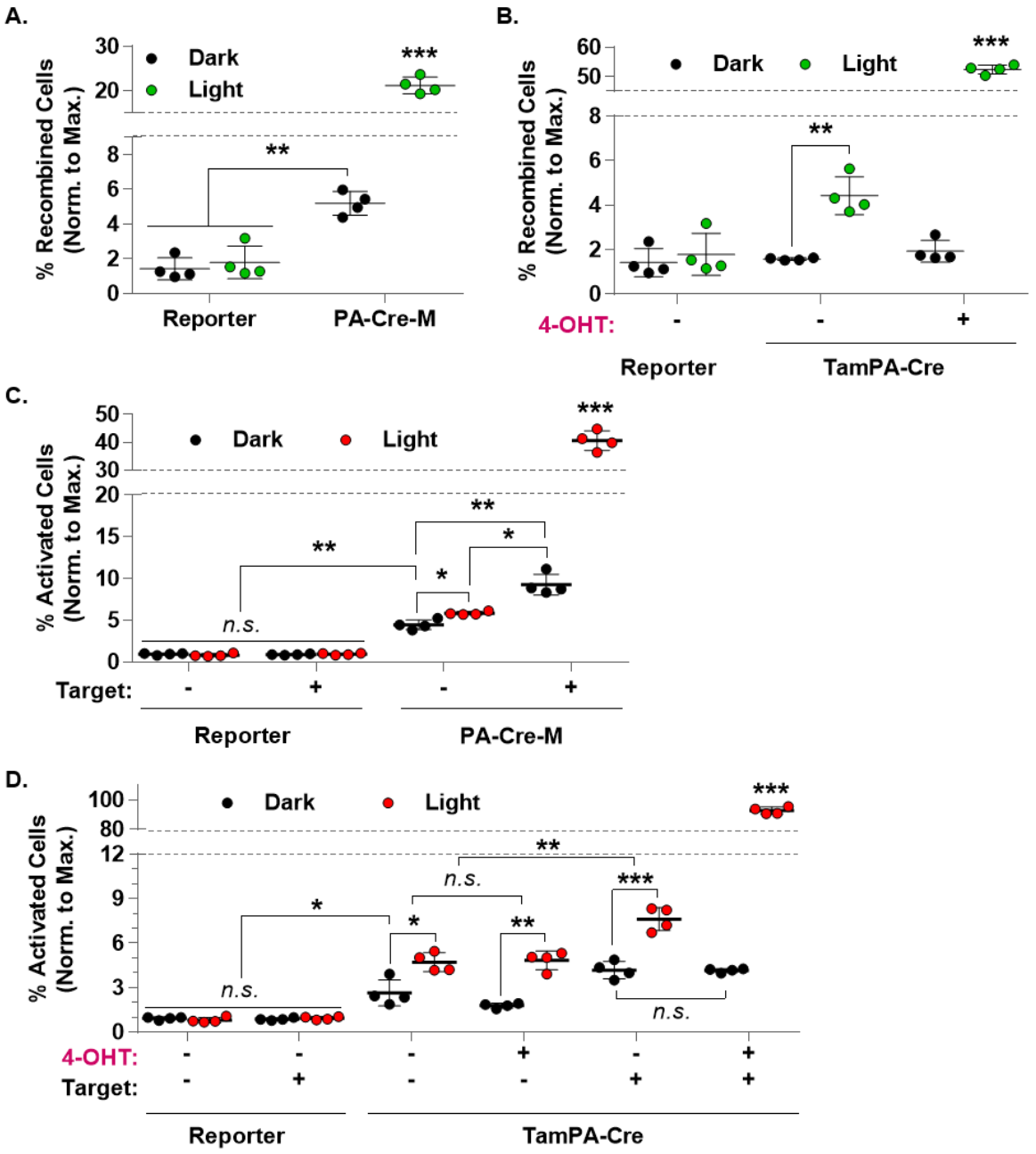

Figure S10. Expanded lower range of plots in Fig. 5B-E. S10A = 5B, S10B = 5C, S10C = 5D, S10D = 5E. Percentage of recombined Jurkat T cells (normalized to maximal recombination) = 100%*(% of CAR-EGFP$^+$ cells) / (initial % of CAR Reporter$^+$ cells, measured via myc). Percentage of activated Jurkat T cells (normalized to maximal recombination) = 100%*(% of CD69$^+$ cells) / (initial % of CAR Reporter$^+$ cells, measured via myc).

SI References

1. Wu, C. Y.; Roybal, K. T.; Puchner, E. M.; Onuffer, J.; Lim, W. A., Remote control of therapeutic T cells through a small molecule-gated chimeric receptor. *Science* **2015,** *350* (6258).
2. Kloss, C. C.; Condomines, M.; Cartellieri, M.; Bachmann, M.; Sadelain, M., Combinatorial antigen recognition with balanced signaling promotes selective tumor eradication by engineered T cells. *Nat Biotechnol* **2013,** *31* (1), 71-+.
3. Roybal, K. T.; Rupp, L. J.; Morsut, L.; Walker, W. J.; McNally, K. A.; Park, J. S.; Lim, W. A., Precision Tumor Recognition by T Cells With Combinatorial Antigen-Sensing Circuits. *Cell* **2016,** *164* (4), 770-9.
4. Taslimi, A.; Zoltowski, B.; Miranda, J. G.; Pathak, G. P.; Hughes, R. M.; Tucker, C. L., Optimized second-generation CRY2-CIB dimerizers and photoactivatable Cre recombinase. *Nat Chem Biol* **2016,** *12* (6), 425-30.
5. Kawano, F.; Okazaki, R.; Yazawa, M.; Sato, M., A photoactivatable Cre-loxP recombination system for optogenetic genome engineering. *Nat Chem Biol* **2016,** *12* (12), 1059-+.
6. Komatsubara, A. T.; Matsuda, M.; Aoki, K., Quantitative analysis of recombination between YFP and CFP genes of FRET biosensors introduced by lentiviral or retroviral gene transfer. *Sci Rep* **2015,** *5*, 13283.
7. Kawano, F.; Suzuki, H.; Furuya, A.; Sato, M., Engineered pairs of distinct photoswitches for optogenetic control of cellular proteins. *Nat Commun* **2015,** *6*, 6256.